Figure 1 Photographs of patient #23 with UPD(14)pat and patient #27 with epimutation.

appeared to be specific to UPD(14)pat and related conditions, and were recognizable from infancy through childhood.

Thoracic abnormality

The 34 patients invariably showed small bell-shaped small thorax with coat-hanger appearance of the ribs in infancy (Figure 2). Long-term (≥10 years) follow-up in patient #12 of UPD-group and patient #31 of Del-S1 who had ~5 times of *RTL1* expression, and in patient #34 of Del-S3 who had ~2.5 times of *RTL1* expression, showed that the CHAs remained above the normal range of age-matched control children, while the M/W ratios, though they were below the normal range in infancy, became within the normal range after infancy (Figure 2). Laryngomalacia was also often detected in each group.

Mechanical ventilation was performed in all patients except for patients #14 and #20 of UPD-group, and tracheostomy was also carried out in about one-third of patients. Mechanical ventilation could be discontinued during infancy in 22 patients (Supplementary Figure S3). Ventilation duration was variable with a median period of 1 month among the 22 patients, and was apparently unrelated to the underlying genetic cause or gestational age.

Abdominal wall defects

Omphalocele was identified in about one-third of patients, and diastasis recti was found in the remaining patients.

Developmental status

Developmental delay (DD) and/or intellectual disability (ID) was invariably present in 26 patients examined (age, 10 months to 15 years), with the median developmental/intellectual quotient (DQ/IQ) of 55 (range, 29–70) (Figure 3). Gross motor development was also almost invariably delayed, with grossly similar patterns among different groups. In patients who passed gross motor developmental milestones, head control was achieved at ~7 months, sitting without support at ~12 months, and walking without support at ~2.1 years of age.

Other features

Several prevalent features were also identified. In particular, except for patient #22, feeding difficulty with poor sucking and swallowing was exhibited by all patients who were affected with polyhydramnios, and gastric tube feeding was performed in all patients who survived more than 1 week (Supplementary Figure S4). Tube-feeding duration was variable with a median period of ~7.5 months in 16 patients for whom tube feeding was discontinued, and tended to be longer in Del-group. In addition, there were several features manifested by single patients (Supplementary Table S2).

Notably, hepatoblastoma was identified at 46 days of age in patient #17, at 218 days in patient #18, and at 13 months of age in patient #8 of UPD-group (Figure 4). It was surgically removed in patients #8 and #18, although chemotherapy was not performed because of poor body condition. In patient #17, neither an operation nor chemotherapy could be carried out because of the patient's severely poor body condition. Histological examination of the removed tumors revealed a poorly differentiated embryonal hepatoblastoma with focal macrotrabecular lesions in patient #8 (Figure 4) and a well-differentiated hepatoblastoma in patient #18.[10]

Mortality

Eight patients were deceased before 4 years of age. The survival rate was 78% in UPD-group, 100% in Epi-group, and 50% in Del-group; it was 25% in patients born ≤29 weeks of gestation, 83% in those born 30–36 weeks of gestation, and 86% in those born ≥37 weeks of gestation (Figure 5). The cause of death was variable; however, respiratory problems were a major factor, because patient #1 died

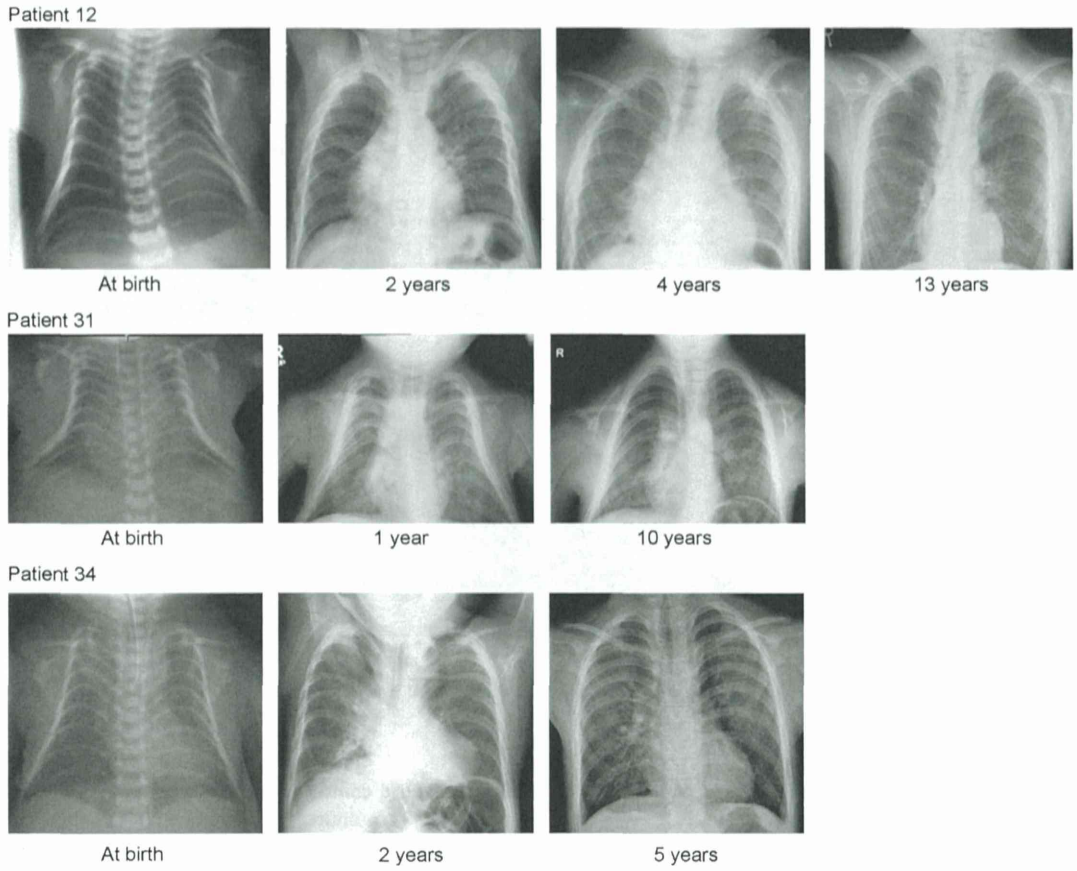

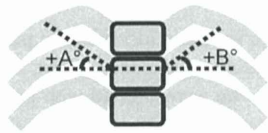

CHA = (A + B) ÷ 2
(6th posterior ribs)

M/W ratio = a / b

		CHA	M/W ratio
Patient 12	At birth	41	70
	2 years	39	88
	4 years	42	94
	13 years	39	92
Patient 31	At birth	35	58
	1 year	28	80
	10 years	29	85
Patient 34	At birth	44	70
	2 year	48	93
	5 years	37	96
UPD(14)pat	At birth	+28 ~ +45	58 ~ 80 (n=8)
	~ 5 years	+25 ~ +45	>78% (n=3)
Controls	At birth	–11 ~ +1.9	82 ~ 89 (n=10)
	~ 5 years	–21 ~ +15	83 ~ 98 (n=10)
	~ 10 years	–9.3 ~ +20	91 ~ 100 (n=10)

Figure 2 Chest roentgenograms of patient #12 of UPD-group, patient #31 of Del-S1, and patient #34 of Del-S3. *RTL1* expression level is predicted to be ~5 times higher in patients #12 and #31, and ~2.5 times higher in patient #34. The CHA to the ribs remains above the normal range throughout the study period, whereas the M/W ratio (the ratio of the mid to widest thorax diameter) normalizes with age.

of neonatal respiratory distress syndrome, and patients #8, #30 and #33 died during a respiratory infection. Of the three patients with hepatoblastoma, patient #17 died of hepatoblastoma, whereas patient #8 died during influenza infection and patient #18 died of hemophagocytic syndrome.

Comparison among/between different groups/subtypes

Clinical findings were grossly similar among/between different groups/subtypes with different expression dosages of *RTL1* and *DLK1*. However, significant differences were found for short gestational age and long duration of tube feeding in Del-group (among three groups

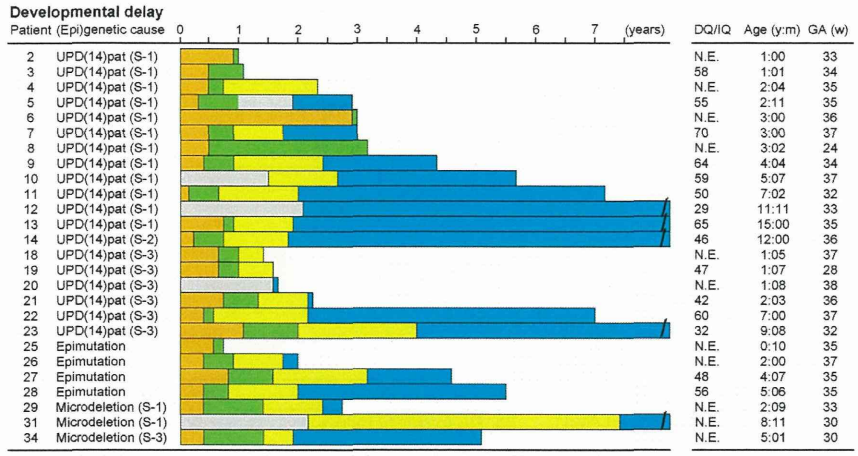

Figure 3 Developmental status. The orange, green, yellow, and blue bars represent the period before head control, the period after head control and before sitting without support, the period after sitting without support and before walking without support, and the period after walking without support, respectively. The gray bars denote the period with no information. DQ, developmental quotient; IQ, intellectual quotient; N.E., not examined; Age, age at the last examination or at death; and GA, gestational age.

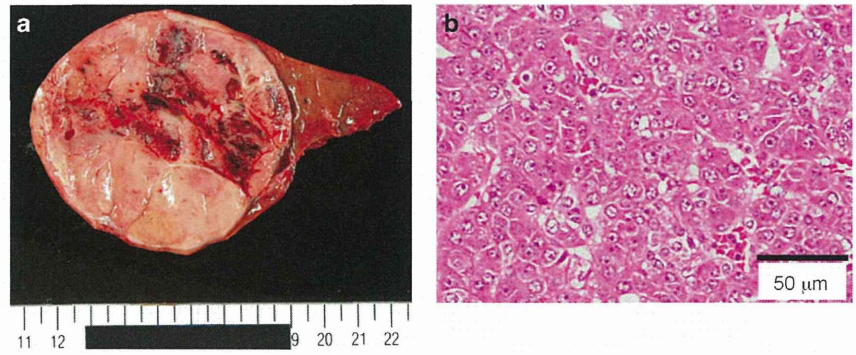

Figure 4 Hepatoblastoma in patient #8 of UPD-group. (**a**) Macroscopic appearance of the hepatoblastoma with a diameter of ~8 cm. (**b**) Microscopic appearance of the hepatoblastoma exhibiting a trabecular pattern. The hepatoblastoma cells are associated with eosinophilic cytoplasm and large nuclei, and resemble fetal hepatocytes.

and against Epi-group and UPD-group) and infrequent hairy forehead in Epi-group (among three groups and against UPD-group) (actual *P*-values are available on request).

DISCUSSION

We examined detailed clinical findings in patients with UPD(14)pat and related conditions. The results indicate that the facial features with full cheeks and protruding philtrum and the thoracic roentgenographic findings with increased CHAs to the ribs represent the pathognomonic features of UPD(14)pat and related conditions from infancy through the childhood. In addition, the decreased M/W ratios also denote the diagnostic hallmark in infancy, but not after infancy. Although other features such as polyhydramnios, placentomegaly, and abdominal wall defects are characteristic of UPD(14)pat and related conditions, they would be regarded as rather nonspecific features that are also observed in other conditions such as Beckwith–Wiedemann syndrome (BWS) (Supplementary Table S4).[12,13]

Such body and placental features were similarly exhibited by patients of each group/subtype, including those of Del-S1, Del-S2, and Del-S3 with different expression dosage of *DLK1* (1× or 2×) and *RTL1* (~2.5× or ~5×), except for patient #32 of Del-S2 who showed typical body features but apparently lacked placental features. Indeed, the difference in the *DLK1* expression dosage had no discernible clinical effects, although mouse *Dlk1* is expressed in several fetal tissues, including the ribs.[14,15] Similarly, in contrast to our previous report which suggested a possible dosage effect of *RTL1* expression level on the phenotypic severity,[2] the difference in the *RTL1* expression dosage turned out to have no recognizable clinical effects after analyzing long-term clinical courses in the affected patients. This suggests that ~2.5×*RTL1* expression is the primary factor for the phenotypic development in the body and placenta. Consistent with the critical role of excessive *RTL1* expression in the phenotypic development, mouse *Rtl1* is clearly expressed in the fetal ribs and skeletal muscles (Supplementary Figure S5) as well as in the placenta,[16,17] and human *RTL1* mRNA and RTL1 protein are strongly expressed in placentas with UPD(14)pat.[6] Thus, lack of placental abnormalities in patient #32 can be explained by assuming a positive *RTL1as* expression and resultant normal (1×) *RTL1* expression in the placenta (Supplementary Figure S1). In addition, since mouse *Gtl2* (*Meg3*) is expressed in multiple fetal tissues including the primordial cartilage,[14] this may argue for the positive role of absent *MEGs* expression in phenotypic development.

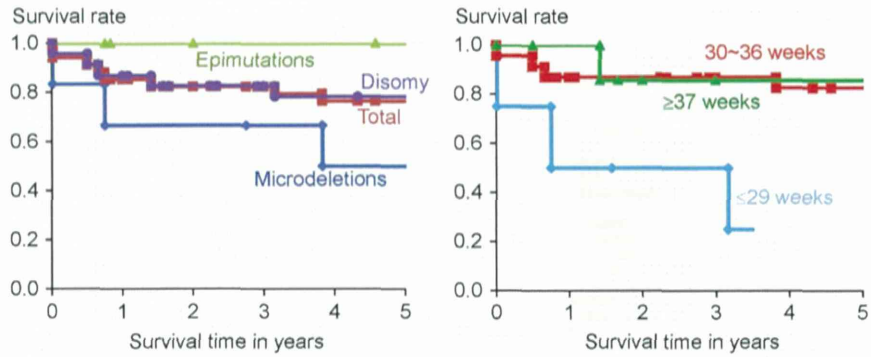

Patient	(Epi)genetic cause	GA	Cause of death	Age of death
1	UPD(14)pat (S-1)	34	Respiratory failure	2 hours
8	UPD(14)pat (S-1)	24	Influenza infection	3 2/12 yrs
15	UPD(14)pat (S-3)	34	Necrotizing enterocolitis	6 mos
17	UPD(14)pat (S-3)	32	Hepatoblastoma	8 mos
18	UPD(14)pat (S-3)	37	Hemophagocytic syndrome	1 5/12 yrs
30	Microdeletion (S-1)	27	Sudden death at URI	9 mos
32	Microdeletion (S-2)	28	Intracranial hemorrhage	4 days
33	Microdeletion (S-3)	35	RS virus infection	3 10/12 yrs

Figure 5 Kaplan–Meier survival curves according to the (epi)genetic cause and the gestational age (week), and summary of the causes of death. GA, gestational age; URI, upper respiratory infection; and RS, respiratory syncytial. Patients #8, #17, and #18 had hepatoblastoma.

The present study revealed several notable findings. First, polyhydramnios was identified during the pregnancies of nearly all patients, except for patient #32 of Del-S2. Amniotic fluid originates primarily from fetal urine and is absorpted primarily by fetal swallowing into the digestive system.[18,19] Since fetal hydration and the resultant urine flow mainly depend on the water flow from maternal circulation across the placenta,[19] placentomegaly would have facilitated the production of amniotic fluid. Furthermore, since feeding difficulty with impaired swallowing was observed in most patients, defective swallowing would have compromised absorption of amniotic fluid. Thus, both body and placental factors are assumed for the development of polyhydramnios. This would explain why polyhydramnios was observed in patients #1, #6, and #8 who were free from placentomegaly, and in patient #22 who showed no feeding difficulty, although the presence of feeding difficulty was unknown for patient #1 as was placentomegaly for patient #22. In addition, since amniotic fluid begins to increase from 8–11 weeks of gestation and reaches its maximum volume around 32 weeks of gestation,[18,19] this would explain why amnioreduction was usually required from 30 weeks of gestation.

Second, birth size was relatively well preserved, whereas postnatal growth was rather compromised. The well preserved prenatal growth in apparently compromised intrauterine environments would be consistent with the conflict theory that overexpression of *PEGs* promotes fetal and placental growth.[20] Notably, birth weight was disproportionately greater than birth length in the apparent absence of generalized edema. In this regard, mouse *Dlk1*, *Rtl1*, and *Gtl2* (*Meg3*) on the distal part of chromosome 12 are expressed in skeletal muscles (Supplementary Figure S5),[14,17] and paternal disomy for chromosome 12 causes muscular hypertrophy.[21] Thus, patients with UPD(14)pat and related conditions may have muscular hypertrophy especially in the fetal life. The compromised postnatal growth would primarily be because of poor nutrition caused by feeding difficulties, whereas relative overweight suggestive of possible muscular hypertrophy remains to be recognized.

Third, DD/ID was invariably present in all 26 patients examined for their developmental/intellectual status, with the median DQ/IQ of 55. In this regard, mouse *Dlk1*, *Rtl1*, and *Gtl2* (*Meg3*) are expressed in the brain during embryogenesis (Supplementary Figure S5),[22] and *Dlk1* is involved in the differentiation of midbrain dopaminergic neurons.[22] Thus, DD/ID would primarily be ascribed to the altered expression dosage of *PEGs/MEGs* in the brain.

Fourth, hepatoblastoma was identified in three patients of UPD-group during infancy. In this context, it has been reported that (1) mouse *Dlk1*, *Rtl1*, and *Meg3* (*Gtl2*) are expressed in the fetal liver, but not in the adult liver; [14,17,23,24] (2) overexpression of *Rtl1* in the adult mouse liver has induced hepatic tumors with high penetrance;[24] (3) *Meg3* functions as a tumor suppressor gene in mice;[25] (4) human *DLK1* is expressed in the hepatocytes of 5–6 weeks old embryos;[26] and (5) human DLK1 protein is upregulated in hepatoblastoma.[27] These findings imply the relevance of excessive *RTL1* expression and loss of *MEG3* expression to the occurrence of hepatoblastoma in UPD(14)pat and related conditions, while it remains to be determined whether the DLK1 upregulation is the cause or the result of hepatoblastoma development. Thus, periodical screening for hepatoblastoma, such as serum α-fetoprotein measurement and abdominal ultrasonography, is recommended. In this context, it remains to be studied whether other embryonal tumors may also be prone to occur in UPD(14)pat and related conditions.

Fifth, mortality was high in Del-group and null in Epi-group. The high mortality in Del-group would primarily be ascribed to the high prevalence of premature delivery, although it is unknown whether the high prevalence of premature delivery is an incidental finding or characteristic of Del-group. The null mortality in Epi-group may be due to possible mosaicism with cells accompanied by a normal expression pattern because of escape from epimutation, as reported previously.[28,29] It is unknown, however, whether possible presence of trisomic cells in TR-mediated UPD(14)pat and that of normal cells in PE-mediated UPD(14) may have exerted clinical effects. Notably, since

death was observed only in patients <4 years of age, the vital prognosis is expected to be good from childhood. In addition, since three patients died during respiratory infections, careful management is recommended during such infections.

Furthermore, the present study also provides several useful clinical implications: (1) two patients had Robertsonian translocations as a risk factor for the development of UPD.[30] Thus, karyotyping is suggested for patients with an UPD(14)pat-like phenotype; (2) prenatal detection of polyhydramnios and thoracic and abdominal features is possible from ~25 weeks of gestation; (3) mechanical ventilation and gastric tube feeding are usually required, with variable durations; (4) there was no patient in UPD-group who exhibited clinical features that are attributable to the unmasking of a recessive mutation(s) of paternal origin; (5) since UPD(14)pat and related conditions share several clinical features including embryonal tumors with BWS (Supplementary Table S4), UPD(14)pat and related conditions may be worth considering in atypical or underlying factor-unknown BWS; and (6) since clinical findings are comparable between patients examined in this study and 17 similarly affected non-Japanese patients (Supplementary Table S5), our data will be applicable to non-Japanese patients as well.

A critical matter for UPD(14)pat and related conditions is the lack of a syndrome name. Although the term 'UPD(14)pat syndrome' has been utilized previously,[4] the term is confusing because 'UPD(14)pat syndrome' can be caused by (epi)genetic mechanisms other than UPD (14)pat. In this regard, the name 'Temple syndrome' has been proposed for UPD(14)mat and related conditions or 'UPD(14)mat syndrome',[31,32] a mirror image of UPD(14)pat and related conditions. On the basis of our previous and present studies that have made a significant contribution to the clarification of underlying (epi)genetic factors and the definition of clinical findings, we would propose the name 'Kagami–Ogata syndrome', or 'Wang–Kagami–Ogata syndrome' with the name of Wang who first described UPD(14)pat,[33] for UPD (14)pat and related conditions.

In summary, although the number of patients still remains small, especially in each subtype of Del-group, the present study reveals pathognomic and characteristic clinical findings in UPD(14)pat and related conditions. Furthermore, this study shows the invariable occurrence of DD/ID and the occasional (8.8%) development of hepatoblastoma, thereby showing the necessity of adequate support for DD/ID and screening of hepatoblastoma in affected patients. Finally, we propose the name 'Kagami–Ogata syndrome' for UPD(14)pat and related conditions.

CONFLICT OF INTEREST

The authors declare no conflict of interest.

ACKNOWLEDGEMENTS

We are grateful to all patients and their parents for their cooperation. We thank Drs Haruhiko Sago, Aiko Sasaki, Jun Shibasaki, Rika Kosaki, Michiko Hayashidani, Toshio Takeuchi, Shinya Tanaka, Mika Noguchi, Goro Sasaki, Kouji Matsumoto, Takeshi Utsunomiya, Yumiko Komatsu, Hirofumi Ohashi, Hiroshi Kishimoto, Maureen J O'Sullivan, Andrew J Green, Yoshiyuki Watabe, Tsuyako Iwai, Hitoshi Kawato, Akiko Yamamoto, Nobuhiro Suzumori, Hiroko Ueda, Makoto Kuwajima, Kiyoko Samejima, Hiroshi Yoshihashi, Yoriko Watanabe, Jin Nishimura, Shuku Ishikawa, Michiko Yamanaka, Machiko Nakagawa, Hiroharu Inoue, Takashi Imamura, Keiichi Motoyama and Ryoko Yoshinare for providing us with detailed clinical data and materials for molecular studies, Dr Gen Nishimura for interpretation of roentgengraphic findings, and Drs Tadayuki Ayabe, Keiko Matsubara, Yoichi Sekita and Maki Fukami for their support in molecular analyses. We also thank Ms. Emma Barber for her editorial assistance with the final draft of this paper. This work was supported by: Grants-in-Aid for Scientific Research (A) (25253023) and Research (B) (23390083) from the Japan Society for the Promotion of Science (JSPS), and by Grants for Health Research on Children, Youth, and Families (H25-001) and for Research on Intractable Diseases (H22-161) from the Ministry of Health, Labor and Welfare (MHLW), by Grants from the National Center for Child Health and Development (23A-1, 25-10), and by a Grant from Takeda Science Foundation.

1 da Rocha ST, Edwards CA, Ito M, Ogata T, Ferguson-Smith AC: Genomic imprinting at the mammalian Dlk1-Dio3 domain. *Trends Genet* 2008; **24**: 306–316.
2 Kagami M, Sekita Y, Nishimura G *et al*: Deletions and epimutations affecting the human 14q32.2 imprinted region in individuals with paternal and maternal upd(14)-like phenotypes. *Nat Genet* 2008; **40**: 237–242.
3 Kagami M, O'Sullivan MJ, Green AJ *et al*: The IG-DMR and the MEG3-DMR at human chromosome 14q32.2: hierarchical interaction and distinct functional properties as imprinting control centers. *PLoS Genet* 2010; **6**: e1000992.
4 Beygo J, Elbracht M, de Groot K *et al*: Novel deletions affecting the MEG3-DMR provide further evidence for a hierarchical regulation of imprinting in 14q32. *Eur J Hum Genet* 2015; **23**: 180–188.
5 Hoffmann K, Heller R: Uniparental disomies 7 and 14. *Best Pract Res Clin Endocrinol Metab* 2011; **25**: 77–100.
6 Kagami M, Matsuoka K, Nagai T *et al*: Paternal uniparental disomy 14 and related disorders: placental gene expression analyses and histological examinations. *Epigenetics* 2012; **7**: 1142–1150.
7 Kurosawa K, Sasaki H, Sato Y *et al*: Paternal UPD14 is responsible for a distinctive malformation complex. *Am J Med Genet* 2002; **110**: 268–272.
8 Kagami M, Nishimura G, Okuyama T *et al*: Segmental and full paternal isodisomy for chromosome 14 in three patients: narrowing the critical region and implication for the clinical features. *Am J Med Genet A* 2005; **138A**: 127–132.
9 Kagami M, Kato F, Matsubara K, Sato T, Nishimura G, Ogata T: Relative frequency of underlying genetic causes for the development of UPD(14)pat-like phenotype. *Eur J Hum Genet* 2012; **20**: 928–932.
10 Horii M, Horiuchi H, Momoeda M, Nakagawa M *et al*: Hepatoblastoma in an infant with paternal uniparental disomy 14. *Congenit Anom (Kyoto)* 2012; **52**: 219–220.
11 Miyazaki O, Nishimura G, Kagami M, Ogata T: Radiological evaluation of dysmorphic thorax of paternal uniparental disomy 14. *Pediatr Radiol* 2011; **41**: 1013–1019.
12 Parveen Z, Tongson-Ignacio JE, Fraser CR, Killeen JL, Thompson KS: Placental mesenchymal dysplasia. *Arch Pathol Lab Med* 2007; **131**: 131–137.
13 Williams DH, Gauthier DW, Maizels M: Prenatal diagnosis of Beckwith–Wiedemann syndrome. *Prenat Diagn* 2005; **25**: 879–884.
14 da Rocha ST, Tevendale M, Knowles E, Takada S, Watkins M, Ferguson-Smith AC: Restricted co-expression of Dlk1 and the reciprocally imprinted non-coding RNA, Gtl2: implications for cis-acting control. *Dev Biol* 2007; **306**: 810–823.
15 da Rocha ST, Charalambous M, Lin SP *et al*: Gene dosage effects of the imprinted delta-like homologue 1 (dlk1/pref1) in development: implications for the evolution of imprinting. *PLoS Genet* 2009; **5**: e1000392.
16 Sekita Y, Wagatsuma H, Nakamura K *et al*: Role of retrotransposon-derived imprinted gene, Rtl1, in the feto-maternal interface of mouse placenta. *Nat Genet* 2008; **40**: 243–248.
17 Brandt J, Schrauth S, Veith AM *et al*: Transposable elements as a source of genetic innovation: expression and evolution of a family of retrotransposon-derived neogenes in mammals. *Gene* 2005; **345**: 101–111.
18 Modena AB, Fieni S: Amniotic fluid dynamics. *Acta Biomed* 2004; **75**: 11–13.
19 Beall MH, van den Wijngaard JP, van Gemert MJ, Ross MG: Amniotic fluid water dynamics. *Placenta* 2007; **28**: 816–823.
20 Hurst LD, McVean GT: Growth effects of uniparental disomies and the conflict theory of genomic imprinting. *Trends Genet* 1997; **13**: 436–443.
21 Georgiades P, Watkins M, Surani MA, Ferguson-Smith AC: Parental origin-specific developmental defects in mice with uniparental disomy for chromosome 12. *Development* 2000; **127**: 4719–4728.
22 Wilkinson LS, Davies W, Isles AR: Genomic imprinting effects on brain development and function. *Nat Rev Neurosci* 2007; **8**: 832–843.
23 Kang ER, Iqbal K, Tran DA *et al*: Effects of endocrine disruptors on imprinted gene expression in the mouse embryo. *Epigenetics* 2011; **6**: 937–950.
24 Riordan JD, Keng VW, Tschida BR *et al*: Identification of rtl1, a retrotransposon-derived imprinted gene, as a novel driver of hepatocarcinogenesis. *PLoS Genet* 2013; **9**: e1003441.
25 Zhou Y, Zhang X, Klibanski A: MEG3 noncoding RNA: a tumor suppressor. *J Mol Endocrinol* 2012; **48**: R45–R53.
26 Floridon C, Jensen CH, Thorsen P *et al*: Does fetal antigen 1 (FA1) identify cells with regenerative, endocrine and neuroendocrine potentials? A study of FA1 in embryonic, fetal, and placental tissue and in maternal circulation. *Differentiation* 2000; **66**: 49–59.
27 Falix FA, Aronson DC, Lamers WH, Hiralall JK, Seppen J: DLK1, a serum marker for hepatoblastoma in young infants. *Pediatr Blood Cancer* 2012; **59**: 743–745.
28 Yamazawa K, Kagami M, Fukami M, Matsubara K, Ogata T: Monozygotic female twins discordant for Silver-Russell syndrome and hypomethylation of the H19-DMR. *J Hum Genet* 2008; **53**: 950–955.

29 Azzi S, Blaise A, Steunou V *et al*: Complex tissue-specific epigenotypes in Russell–Silver Syndrome associated with 11p15 ICR1 hypomethylation. *Hum Mutat* 2014; **35**: 1211–1220.
30 Berend SA, Horwitz J, McCaskill C, Shaffer LG: Identification of uniparental disomy following prenatal detection of Robertsonian translocations and isochromosomes. *Am J Hum Genet* 2000; **66**: 1787–1793.
31 Ioannides Y, Lokulo-Sodipe K, Mackay DJ, Davies JH, Temple IK: Temple syndrome: improving the recognition of an underdiagnosed chromosome 14 imprinting disorder: an analysis of 51 published cases. *J Med Genet* 2014; **51**: 495–501.
32 Hosoki K, Kagami M, Tanaka T *et al*: Maternal uniparental disomy 14 syndrome demonstrates Prader–Willi syndrome-like phenotype. *J Pediatr* 2009; **155**: 900–903.
33 Wang JC, Passage MB, Yen PH, Shapiro LJ, Mohandas TK: Uniparental heterodisomy for chromosome 14 in a phenotypically abnormal familial balanced 13/14 Robertsonian translocation carrier. *Am J Hum Genet* 1991; **48**: 1069–1074.
34 Kagami M, Yamazawa K, Matsubara K *et al*: Placentomegaly in paternal uniparental disomy for human chromosome 14. *Placenta* 2008; **29**: 760–761.

Supplementary Information accompanies this paper on European Journal of Human Genetics website (http://www.nature.com/ejhg)

nature COMMUNICATIONS

ARTICLE

Received 24 Jan 2014 | Accepted 2 Oct 2014 | Published 14 Nov 2014

DOI: 10.1038/ncomms6464 OPEN

The role of maternal-specific H3K9me3 modification in establishing imprinted X-chromosome inactivation and embryogenesis in mice

Atsushi Fukuda[1], Junko Tomikawa[2], Takumi Miura[1], Kenichiro Hata[2], Kazuhiko Nakabayashi[2], Kevin Eggan[3], Hidenori Akutsu[1] & Akihiro Umezawa[1]

Maintaining a single active X-chromosome by repressing *Xist* is crucial for embryonic development in mice. Although the *Xist* activator RNF12/RLIM is present as a maternal factor, maternal *Xist* (Xm-*Xist*) is repressed during preimplantation phases to establish imprinted X-chromosome inactivation (XCI). Here we show, using a highly reproducible chromatin immunoprecipitation method that facilitates chromatin analysis of preimplantation embryos, that H3K9me3 is enriched at the *Xist* promoter region, preventing Xm-*Xist* activation by RNF12. The high levels of H3K9me3 at the *Xist* promoter region are lost in embryonic stem (ES) cells, and ES-cloned embryos show RNF12-dependent *Xist* expression. Moreover, lack of Xm-XCI in the trophectoderm, rather than loss of paternally expressed imprinted genes, is the primary cause of embryonic lethality in 70–80% of parthenogenotes immediately after implantation. This study reveals that H3K9me3 is involved in the imprinting that silences Xm-*Xist*. Our findings highlight the role of maternal-specific H3K9me3 modification in embryo development.

[1] Department of Reproductive Biology, National Research Institute for Child Health and Development, 2-10-1 Okura, Setagaya, Tokyo 157-8535, Japan. [2] Department of Maternal-Foetal Biology, National Research Institute for Child Health and Development, 2-10-1 Okura, Setagaya, Tokyo 157-8535, Japan. [3] The Howard Hughes Medical Institute, Harvard Stem Cell Institute and the Department of Stem Cell and Regenerative Biology, Harvard University, 7 Divinity Avenue, Cambridge, Massachusetts 02138, USA. Correspondence and requests for materials should be addressed to H.A. (email: akutsu-h@ncchd.go.jp).

To maintain proper dosage compensation in mammals, one of the two X chromosomes in the female is inactivated[1,2]. In establishment of X-chromosome inactivation (XCI), a large non-coding RNA, *Xist*, is expressed and this non-coding RNA then covers the entire X chromosome in *cis*[1–3]. In mice, two types of XCI occur during female embryonic development. One type involves random XCI, which is observed in cells derived from epiblasts, and one of the two X chromosomes (paternal or maternal) is randomly inactivated. The other involves imprinted XCI (iXCI), which is observed in extra-embryonic tissues and causes XCI of the paternal X chromosome (Xp)[4]. The initiation of iXCI begins at early preimplantation in embryos and Xp-*Xist* is expressed around the four-cell stage[1]. A recent study showed that a maternal factor, the E3 ubiquitin ligase RNF12, is the primary factor responsible for Xp-*Xist* activation[5]. Interestingly, although RNF12 is abundant as a maternal factor in oocytes, Xm-*Xist* is not expressed. Moreover, maternal *Xist* (Xm-*Xist*)-specific imprints, which are refractory to the Xm-*Xist* activation induced by RNF12, are imposed during oogenesis[6]. *Xist* expression analysis using *de novo* DNA methyltransferase (*Dnmt3a/b*) maternal knockout mice demonstrated that *Xist* expression during preimplantation is independent of DNA methylation[7], implying that other epigenetic factors are associated with Xm-*Xist* silencing. However, the nature of these Xm-specific epigenetic modifications is unknown.

A gene-knockout study demonstrated that loss of Xp-*Xist* expression critically affects postimplantation female development due to lack of iXCI, which causes overexpression of X-linked genes in extra-embryonic tissues[8]. Similar to the phenotype observed in Xp-*Xist*-knockout mice, parthenogenetic embryos (PEs) composed of two X chromosomes show increased expression of X-linked genes, as compared with fertilized females, because of the low expression of *Xist*[9]. One of the interesting phenomena observed in PEs is the dramatic developmental failure that occurs immediately after implantation. Around 70–80% of embryos die before embryonic day (E) 9.5, which is the limit of development for PEs[10]. However, it is unknown whether the primary cause of rapid developmental failure in postimplantation PEs is the loss of iXCI or the loss of expression of autosomal paternally imprinted genes[11,12].

The global epigenetic asymmetry of parental genomes in zygotes is retained during early preimplantation phases in mice and changes in gene expression occur in discrete stages to confer totipotency[13,14]. Interestingly, transcriptionally repressive marks, such as histone H3 lysine 9 di-/trimethylation (H3K9me2/3), are specifically imposed on maternal genomes at the zygote stage[13]. Although the regulation of imprinted genes mostly depends on DNA methylation, some imprinted genes are regulated by these histone modifications[15,16]. Thus, Xm-*Xist* silencing machinery may be associated with histone modifications.

Here we reveal that silencing of Xm-*Xist* in preimplantation embryos involves modification of H3K9me3. By using a new chromatin immunoprecipitation (ChIP) method that facilitates chromatin analysis in preimplantation embryos, we show that the *Xist* promoter on the Xm is highly enriched for H3K9me3 at the four-cell stage. This enrichment is lost in the morula and in male embryonic stem (ES) cells. Furthermore, we demonstrate that early loss of H3K9me3 at the *Xist* promoter leads to precocious Xm-*Xist* activation in a Rnf12-dependent manner. Moreover, we demonstrate that establishment of Xm-XCI in the trophectoderm allows PEs to develop at the postimplantation stage without the expression of paternally imprinted genes on autosomes. Therefore, these data indicate that the primary cause of embryonic lethality immediately after implantation in most PEs is loss of XCI rather than loss of the expression of paternally imprinted genes located on autosomes. Our study revealed that silencing of Xm-*Xist* by imprinting to establish iXCI involves H3K9me3, and this finding is expected to resolve the longstanding issues that have limited our general understanding of XCI in mice.

Results

Changes in histone modifications cause Xm-*Xist* derepression. Histone repressive marks, such as H3K9me2/3 and H3K27me3, are specifically imposed on maternal genomes[13]. To investigate the role of maternal-specific modifications in imprinted *Xist* expression, we focused on *Kdm3a* and *Kdm4b*, which encode histone demethylases specific for H3K9me1/2 and H3K9me3 (refs 17,18), respectively. Reverse transcription–PCR analysis showed that oocytes express low levels of *Kdm3a* and *Kdm4b* (Supplementary Fig. 1). Immunofluorescence (IF) analyses revealed that zygotes injected with polyadenylated *Kdm3a* and *Kdm4b* messenger RNAs expressed significantly lower levels of maternal H3K9me2 and H3K9me3, respectively (Fig. 1a–d). Ectopic expression of *Kdm3a* and *Kdm4b* did not affect H3K9me3 or H3K9me2 marks, respectively (Supplementary Fig. 2). We reasoned that if Xm-specific modifications that prevent *Xist* activation were erased by these epigenetic modifiers, Xm-*Xist* would be expressed at the four-cell stage, which is when Xp-*Xist* expression commences.

To facilitate analysis of Xm-*Xist* expression, we used PEs (Fig. 1e). PEs possess two copies of Xm, and Xm-*Xist* is never expressed at the four-cell stage[19]. Xm-*Xist* expression in four-cell PEs, cultured for 48 h, was determined using quantitative real-time PCR (qPCR). Consistent with a previous report[19], Xm-*Xist* was not detectably expressed in most intact (not injected) PEs and PEs injected with *Egfp* mRNA (*Egfp*-PEs; Fig. 1f). Approximately 75% of PEs injected with *Kdm3a* mRNA (*Kdm3a*-PEs) did not detectably express *Xist*. However, Xm-*Xist* expression was detected in all PEs injected with *Kdm4b* mRNA (*Kdm4b*-PEs;

Figure 1 | Alterations in histone modifications derepress Xm-*Xist* expression. (**a**–**d**) Oocytes injected with *Kdm3a* (**a**,**b**), *Kdm4b* (**c**,**d**) or *Egfp* mRNAs were subjected to ICSI. After 7–8 h, embryos were fixed and analysed for H3K9me2 (**a**) and H3K9me3 (**c**) using IF. Nuclei stained with 4′,6-diamidino-2-phenylindole (DAPI) are shown in blue. Representative images are presented on the left. The box-and-whisker plot shows the ratio of maternal to paternal signal intensities. The horizontal line indicates the median. The *P*-values were calculated using the Mann–Whitney *U*-test (*U*-test). Pb, polar body; *n*, number of embryos analysed (**b**,**d**). (**e**) Schema of the generation of PEs with altered histone modifications. To examine the effects of histone demethylation on Xm-*Xist* expression, either H3K9me2 demethylase (*Kdm3a*) or H3K9me3 demethylase (*Kdm4b*) mRNAs were injected into MII oocytes that were then activated. To assess the effects of inhibition of histone deacetylation on Xm-*Xist* expression, oocytes were activated and incubated in the presence of TSA for 24 h. After 48 h, ten four-cell PEs were pooled and analysed as one biological replicate using qPCR. (**f**) Analysis of Xm-*Xist* expression at the four-cell stage. The expression level of Xm-*Xist* in female embryos derived from IVF was defined as 1. One or two asterisks indicate Xm-*Xist* expression in one or two replicates, respectively. The *P*-values were determined using Student's *t*-tests. Error bars indicate the mean ± s.e.m. (**g**–**i**) *Xist* FISH analysis of *Kdm4b*- and *Egfp* + TSA-PEs at the four-cell stage. (**g**) Representative images of FISH results. (**h**) Ratio of cells with *Xist* signal to the total number of cells. *n*, number of interphase cells analysed. (**i**) Ratio of cells with biallelic expression to total cells. The detailed FISH results are shown in Supplementary Table 1. Scale bars, 20 μm.

Fig. 1f), suggesting that H3K9me3 demethylation caused Xm-*Xist* derepression.

We next assessed the effects of a histone deacetylase inhibitor, trichostatin A (TSA), on Xm-*Xist* expression. TSA-treated PEs (Intact + TSA-PEs and *Egfp* + TSA-PEs) also activated Xm-*Xist* (Fig. 1f). No significant changes were detected in Xm-*Xist* expression levels between *Kdm4b*-PEs and *Egfp* + TSA-PEs. However, although co-injection with *Kdm4b* and *Kdm3a* mRNAs did not increase Xm-*Xist* expression levels as compared with *Kdm4b*-PEs, a combination of TSA and *Kdm4b*-mRNA significantly increased Xm-*Xist* expression as compared with *Egfp* + TSA-PEs (2.9-fold, $P<0.04$, Student's *t*-test; Fig. 1f). Moreover, derepression of Xm-*Xist* transcription occurred in the absence of *Rnf12* overexpression (Supplementary Fig. 3), and *Jpx* and *Ftx*,

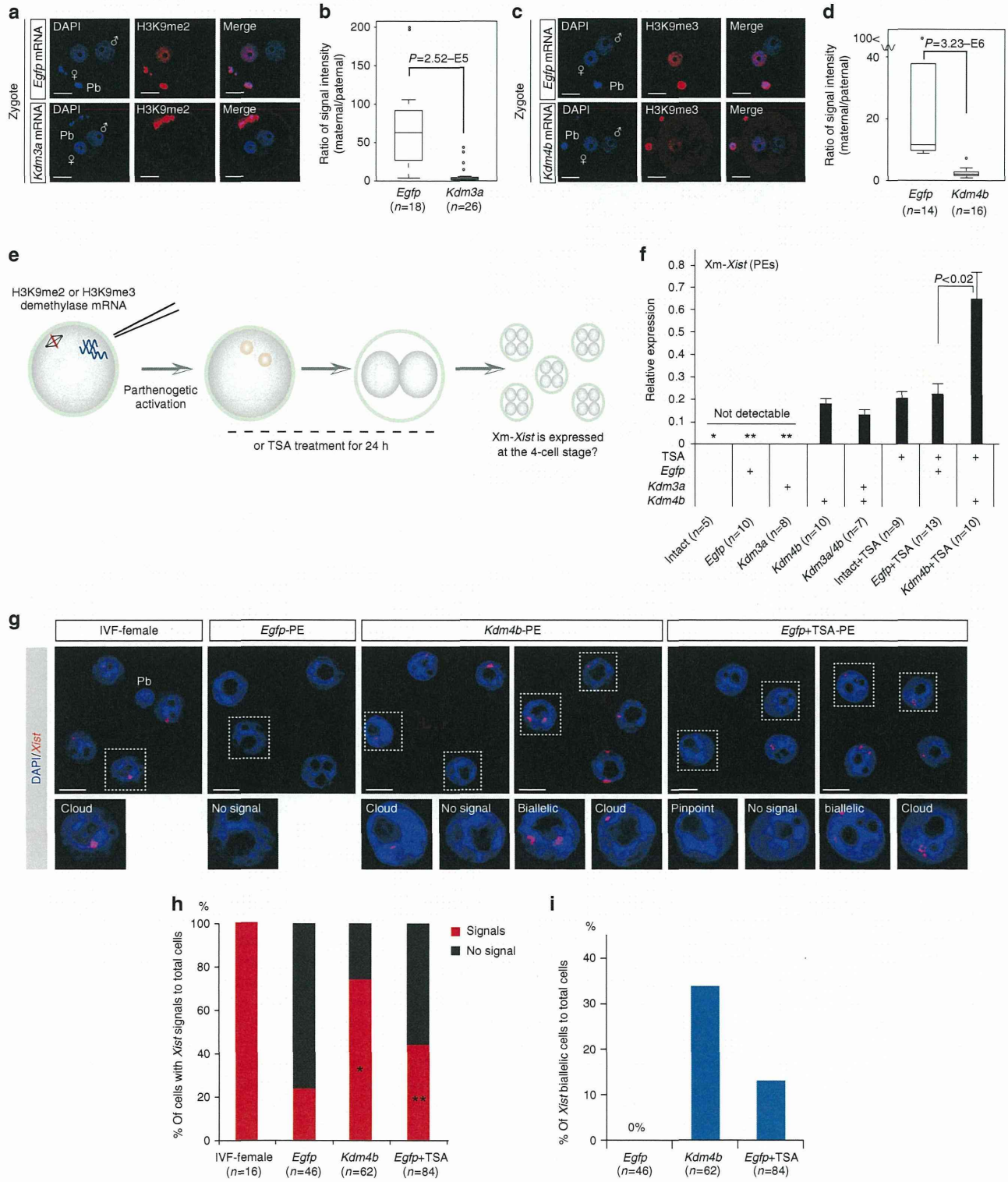

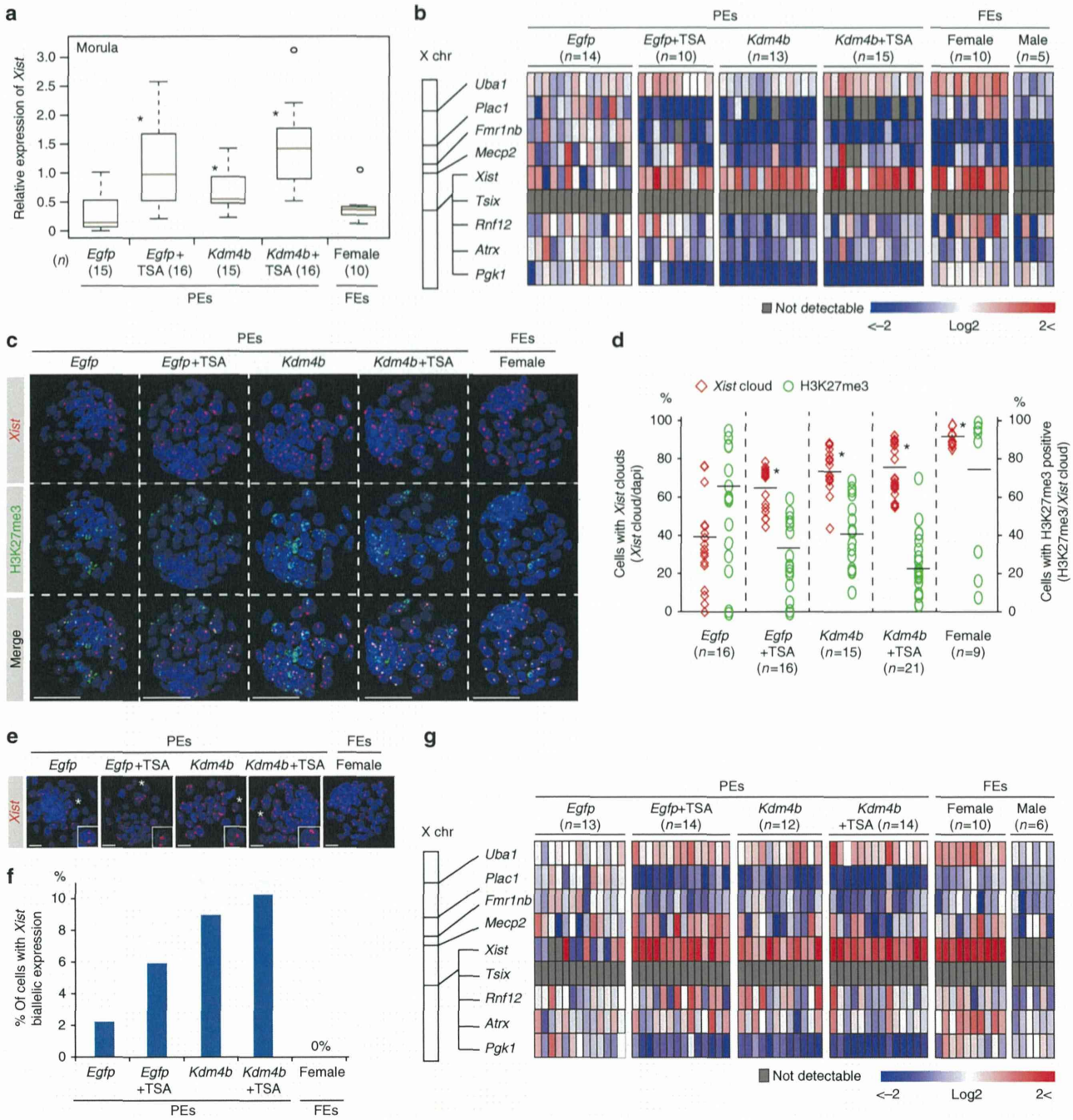

Figure 2 | Global XCI and *Xist* expression states of Xm at late preimplantation stages. (**a**) Analysis of *Xist* expression using qPCR of individual embryos in the morula. An asterisk indicates $P<0.05$ (Student's *t*-test) compared with *Egfp*-PEs. FEs, fertilized embryos. (**b**) Large-scale qPCR analysis of *Xist* and eight X-linked genes in individual blastocysts after culturing for 96 h. Coloured bars indicate expression levels. (**c**,**d**) IF (H3K27me3, green) combined with RNA FISH (*Xist*, red) analysis in 96-h blastocyst stage. 4′,6-diamidino-2-phenylindole (DAPI)-stained nuclei are shown in blue. (**c**) Representative confocal projection. Scale bars, 50 μm. (**d**) The graph shows *Xist* expression and H3K27me3 modification states in individual embryos. The horizontal axis indicates the average percentage in the group. $*P<3.1\times10^{-28}$ (Fisher's exact test). *n*, number of embryos analysed. (**e**,**f**) Xm-*Xist* biallelic expression states in PEs at 96 h. The asterisk indicates cells with biallelic expression. Scale bars, 20 μm. (**f**) Summary of the ratio of biallelic cells to *Xist*-positive cells in 96-h blastocyst stage in each group. The number of cells is shown in Supplementary Table 3. (**g**) qPCR analysis of *Xist* and eight X-linked genes in individual blastocysts after culturing for 120 h. (**h**,**i**) IF (H3K27me3, green) combined with RNA FISH (*Xist*, red) analysis in 120 h blastocysts. $*P<5.4\times10^{-23}$ (Fisher's exact test). Scale bars, 50 μm. (**j**) The ratio of biallelic cells to *Xist*-positive cells in 120 h blastocysts. In qPCR analysis, the average expression level of Xm-*Xist* in *Egfp*-PEs was set as 1 (also see the Methods section). *Gapdh* and *β-actin* were used as internal controls. Data are summarized in Supplementary Table 4.